37. Radioactivity and Radiation Protection

Revised October 2017 by S. Roesler and M. Silari (CERN).

37.1. Definitions [1,2,3]

It would be desirable if legal protection limits could be expressed in directly measurable *physical quantities*. However, this does not allow to quantify biological effects of the exposure of the human body to ionizing radiation.

For this reason, protection limits are expressed in terms of so-called *protection quantities* which, although calculable, are not measurable. Protection quantities quantify the extent of exposure of the human body to ionizing radiation from both whole and partial body external irradiation and from intakes of radionuclides.

In order to demonstrate compliance with dose limits, so-called *operational quantities* are typically used which aim at providing conservative estimates of protection quantities. Often radiation protection detectors used for individual and area monitoring are calibrated in terms of operational quantities and, thus, these quantities become "measurable".

37.1.1. *Physical quantities* :

• **Fluence,** Φ (unit: $1/m^2$): The fluence is the quotient of the sum of the particle trajectory lengths dl in the volume dV

$$\Phi = dl/dV \; . \tag{37.1}$$

It can also be expressed in terms of number of particles dN incident upon a small sphere of cross-sectional area da

$$\Phi = dN/da \; .$$

• **Absorbed dose,** D (unit: gray, 1 Gy=1 J/kg=100 rad): The absorbed dose is the energy imparted by ionizing radiation in a volume element of a specified material divided by the mass of this volume element.

• **Kerma,** K (unit: gray): Kerma is the sum of the initial kinetic energies of all charged particles liberated by indirectly ionizing radiation in a volume element of the specified material divided by the mass of this volume element.

• **Linear energy transfer,** L **or** LET (unit: J/m, often given in keV/μm, 1 keV/μm$\approx$ 1.602×10^{-10} J/m): The linear energy transfer is the mean energy, dE, lost by a charged particle owing to collisions with electrons in traversing a distance dl in matter. *Low-LET radiation:* X rays and gamma rays (accompanied by charged particles due to interactions with the surrounding medium) or light charged particles such as electrons that produce sparse ionizing events far apart at a molecular scale ($L < 10$ keV/μm). *High-LET radiation:* neutrons and heavy charged particles that produce ionizing events densely spaced at a molecular scale ($L > 10$ keV/μm). While the above LET definition refers to electronic stopping power only, at low energy nuclear stopping power could be a significant fraction of the total stopping power.

• **Activity,** A (unit: becquerel, 1 Bq=1/s=27 pCi): Activity is the expectation value of the number of nuclear decays occurring in a given quantity of material per unit time.

37.1.2. *Protection quantities* :

• **Organ absorbed dose,** D_T (unit: gray): The mean absorbed dose in an organ or tissue T of mass m_T is defined as

$$D_T = \frac{1}{m_T} \int_{m_T} D dm \ .$$

• **Equivalent dose,** H_T (unit: sievert, 1 Sv=100 rem): The equivalent dose H_T in an organ or tissue T is equal to the sum of the absorbed doses $D_{T,R}$ in the organ or tissue caused by different radiation types R weighted with so-called radiation weighting factors w_R:

$$H_T = \sum_R w_R \times D_{T,R} \ . \tag{37.2}$$

It expresses long-term risks (primarily cancer and leukemia) from low-level chronic exposure. The values for w_R recommended by ICRP [2] are given in Table 37.1.

Table 37.1: Radiation weighting factors, w_R.

Radiation type	w_R
Photons, electrons and muons	1
Neutrons, $E_n < 1$ MeV	$2.5 + 18.2 \times \exp[-(\ln E_n)^2/6]$
1 MeV $\leq E_n \leq 50$ MeV	$5.0 + 17.0 \times \exp[-(\ln(2E_n))^2/6]$
$E_n > 50$ MeV	$2.5 + 3.25 \times \exp[-(\ln(0.04E_n))^2/6]$
Protons and charged pions	2
Alpha particles, fission fragments, heavy ions	20

• **Effective dose,** E (unit: sievert): The sum of the equivalent doses, weighted by the tissue weighting factors w_T ($\sum_T w_T = 1$) of several organs and tissues T of the body that are considered to be most sensitive [2], is called "effective dose":

$$E = \sum_T w_T \times H_T \ . \tag{37.3}$$

37.1.3. *Operational quantities* :

• **Dose equivalent,** H (unit: sievert): The dose equivalent at a point in tissue is given by:

$$H = D \times Q \tag{37.4}$$

where D is the absorbed dose and Q is the quality factor at that point. The quality factor at a point in tissue, is given by:

$$Q = \frac{1}{D} \int_{L=0}^{\infty} Q(L) D_L dL$$

where D_L is the distribution of D in unrestricted linear energy transfer L at the point of interest, and $Q(L)$ is the quality factor as a function of L. The integration is to be performed over D_L, due to all charged particles, excluding their secondary electrons.

• **Ambient dose equivalent,** $H^*(10)$ (unit: sievert): The dose equivalent at a point in a radiation field that would be produced by the corresponding expanded and aligned field in a 30 cm diameter sphere of unit density tissue (ICRU sphere) at a depth of 10 mm on the radius vector opposing the direction of the aligned field. Ambient dose equivalent is the operational quantity for *area monitoring.*

• **Personal dose equivalent,** $H_p(d)$ (unit: sievert): The dose equivalent in ICRU tissue at an appropriate depth, d, below a specified point on the human body. The specified point is normally taken to be where the individual dosimeter is worn. For the assessment of effective dose, $H_p(10)$ with a depth $d = 10$ mm is chosen, and for the assessment of the dose to the skin and to the hands and feet the personal dose equivalent, $H_p(0.07)$, with a depth $d = 0.07$ mm, is used. Personal dose equivalent is the operational quantity for *individual monitoring.*

37.1.4. *Dose conversion coefficients* :

Dose conversion coefficients allow direct calculation of protection or operational quantities from particle fluence and are functions of particle type, energy and irradiation configuration. The most common coefficients are those for effective dose and ambient dose equivalent. The former are based on simulations in which the dose to organs of anthropomorphic phantoms is calculated for approximate actual conditions of exposure, such as irradiation of the front of the body (antero-posterior irradiation) or isotropic irradiation.

Conversion coefficients from fluence to effective dose are given for anterior-posterior irradiation and various particles in Fig. 37.1 [4]. For example, the effective dose from an anterior-posterior irradiation in a field of 1-MeV neutrons with a fluence of 1 neutron per cm^2 is about 290 pSv. In Monte Carlo simulations such coefficients allow multiplication with fluence at scoring time such that effective dose to a human body at the considered location is directly obtained.
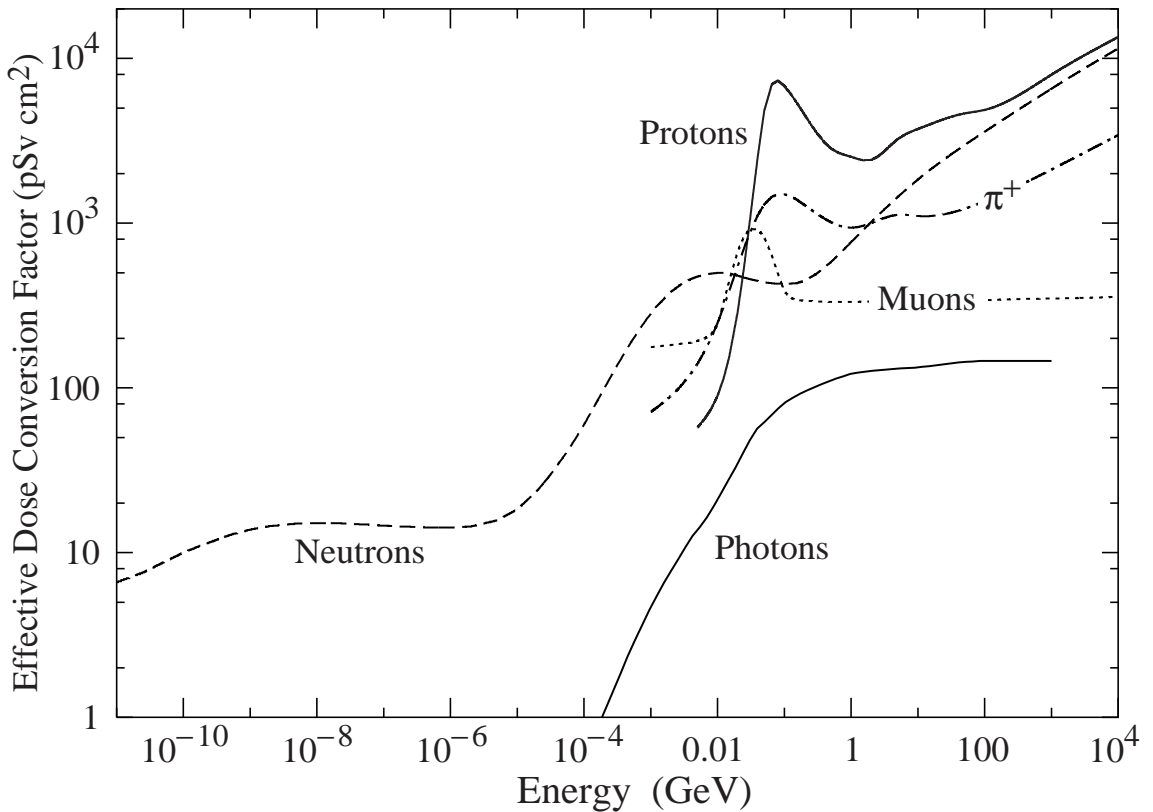
Figure 37.1: Fluence to effective dose conversion coefficients for anterior-posterior irradiation and various particles [4].

37.2. Radiation levels [5]

• **Natural background radiation**: On a worldwide average, the annual whole-body dose equivalent due to all sources of natural background radiation ranges from 1.0 to 13 mSv (0.1–1.3 rem) with an annual average of 2.4 mSv [6]. In certain areas values up to 50 mSv (5 rem) have been measured. A large fraction (typically more than 50%) originates from inhaled natural radioactivity, mostly radon and radon daughters. The latter can vary by more than one order of magnitude: it is 0.1–0.2 mSv in open areas, 2 mSv on average in a house and more than 20 mSv in poorly ventilated mines.

• **Cosmic ray background radiation**: At sea level, the whole-body dose equivalent due to cosmic ray background radiation is dominated by muons; at higher altitudes also nucleons contribute. Dose equivalent rates range from less than 0.1 μSv/h at sea level to a few μSv/h at aircraft altitudes. Details on cosmic ray fluence levels are given in the Cosmic Rays section (Sec. 30 of this *Review*).

37.3. Health effects of ionizing radiation

Radiation can cause two types of health effects, deterministic and stochastic:

• **Deterministic effects** are tissue reactions which cause injury to a population of cells if a given threshold of absorbed dose is exceeded. The severity of the reaction increases with dose. The quantity in use for tissue reactions is the absorbed dose, D. When particles other than photons and electrons (low-LET radiation) are involved, a Relative Biological Effectiveness (RBE)-weighted dose may be used. The RBE of a given radiation is the reciprocal of the ratio of the absorbed dose of that radiation to the absorbed dose of a reference radiation (usually X rays) required to produce the same degree of biological effect. It is a complex quantity that depends on many factors such as cell type, dose rate, fractionation, etc.

• **Stochastic effects** are malignant diseases and heritable effects for which the probability of an effect occurring, but not its severity, is a function of dose without threshold.

• **Lethal dose**: The whole-body dose from penetrating ionizing radiation resulting in 50% mortality in 30 days (assuming no medical treatment) is 2.5–4.5 Gy (250–450 rad)[†], as measured internally on the body longitudinal center line. The surface dose varies due to variable body attenuation and may be a strong function of energy.

• **Cancer induction**: The cancer induction probability is about 5% per Sv on average for the entire population [3].

• **Recommended effective dose limits**: The International Commission on Radiological Protection (ICRP) recommends a limit for radiation workers of 20 mSv effective dose per year averaged over 5 years, with the provision that the dose should not exceed 50 mSv in any single year [3]. The limit in the EU-countries and Switzerland is 20 mSv per year, in the U.S. it is 50 mSv per year (5 rem per year). Many physics laboratories in the U.S. and elsewhere set lower limits. The effective dose limit for general public is typically 1 mSv per year.

37.4. Prompt neutrons at accelerators

Neutrons dominate the particle environment outside thick shielding (*e.g.*, > 1 m of concrete) for high energy ($>$ a few hundred MeV) electron and hadron accelerators. In addition, for accelerators with energies above about 10 GeV, muons contribute significantly at small angles with regard to the beam, even behind several meters of shielding. Another special case are synchrotron light sources where particular care has to be taken to shield the very intense low-energy photons extracted from the electron synchrotron into the experimental areas. Due to its importance at high energy accelerators this section focuses on prompt neutrons.

[†] *RBE*-weighted when necessary

37.4.1.   *Electron accelerators* :

At electron accelerators, neutrons are generated via photonuclear reactions from bremsstrahlung photons. Neutron production takes place above a threshold value which varies from 10 to 19 MeV for light nuclei (with important exceptions, such as 2.23 MeV for deuterium and 1.67 MeV for beryllium) and from 4 to 6 MeV for heavy nuclei. It is commonly described by different mechanisms depending on the photon energy: the giant dipole resonance interactions (from threshold up to about 30 MeV, often the dominant process), the quasi-deuteron effect (between 30 MeV and a few hundred MeV), the delta resonance mechanism (between 200 MeV and a few GeV) and the vector meson dominance model at higher energies.

The giant dipole resonance reaction consists in a collective excitation of the nucleus, in which neutrons and protons oscillate in the direction of the photon electric field. The oscillation is damped by friction in a few cycles, with the photon energy being transferred to the nucleus in a process similar to evaporation. Nucleons emitted in the dipolar interaction have an anisotropic angular distribution, with a maximum at 90°, while those leaving the nucleus as a result of evaporation are emitted isotropically with a Maxwellian energy distribution described as [7]:

$$\frac{dN}{dE_n} = \frac{E_n}{T^2} e^{-E_n/T} \ , \tag{37.5}$$

where T is a nuclear 'temperature' (in units of MeV) characteristic of the particular target nucleus and its excitation energy. For heavy nuclei the 'temperature' generally lies in the range of $T = 0.5$–1.0 MeV. Neutron yields from semi-infinite targets per kW of electron beam power are plotted in Fig. 37.2 as a function of the electron beam energy [7].

While for thick targets neutron production is mainly due to photonuclear interactions, for thin targets (thickness of fractions of the radiation length) electronuclear interactions are the dominating process.

Typical neutron energy spectra outside of concrete (80 cm thick, 2.35 g/cm^3) and iron (40 cm thick) shields are shown in Fig. 37.3. In order to compare these spectra to those caused by proton beams (see below) the spectra are scaled by a factor of 100, which roughly corresponds to the difference in the high energy hadronic cross sections for photons and hadrons (*e.g.*, the fine structure constant). The shape of these spectra are generally characterized by a low-energy peak at around 1 MeV (evaporation neutrons) and a high-energy shoulder at around 70–80 MeV. In case of concrete shielding, the spectrum also shows a pronounced peak at thermal neutron energies.

37.4.2.   *Proton accelerators* :

At proton accelerators, neutron yields emitted per incident proton by different target materials are roughly independent of proton energy between 20 MeV and 1 GeV, and are given by the ratio C : Al : Cu-Fe : Sn : Ta-Pb = 0.3 : 0.6 : 1.0 : 1.5 : 1.7 [10].   Above about 1 GeV, the neutron yield is proportional to E^m, where $0.80 \leq m \leq 0.85$ [11].

Typical neutron energy spectra outside of concrete and iron shielding are shown in Fig. 37.3. Here, the radiation fields are caused by a 25 GeV proton beam interacting with
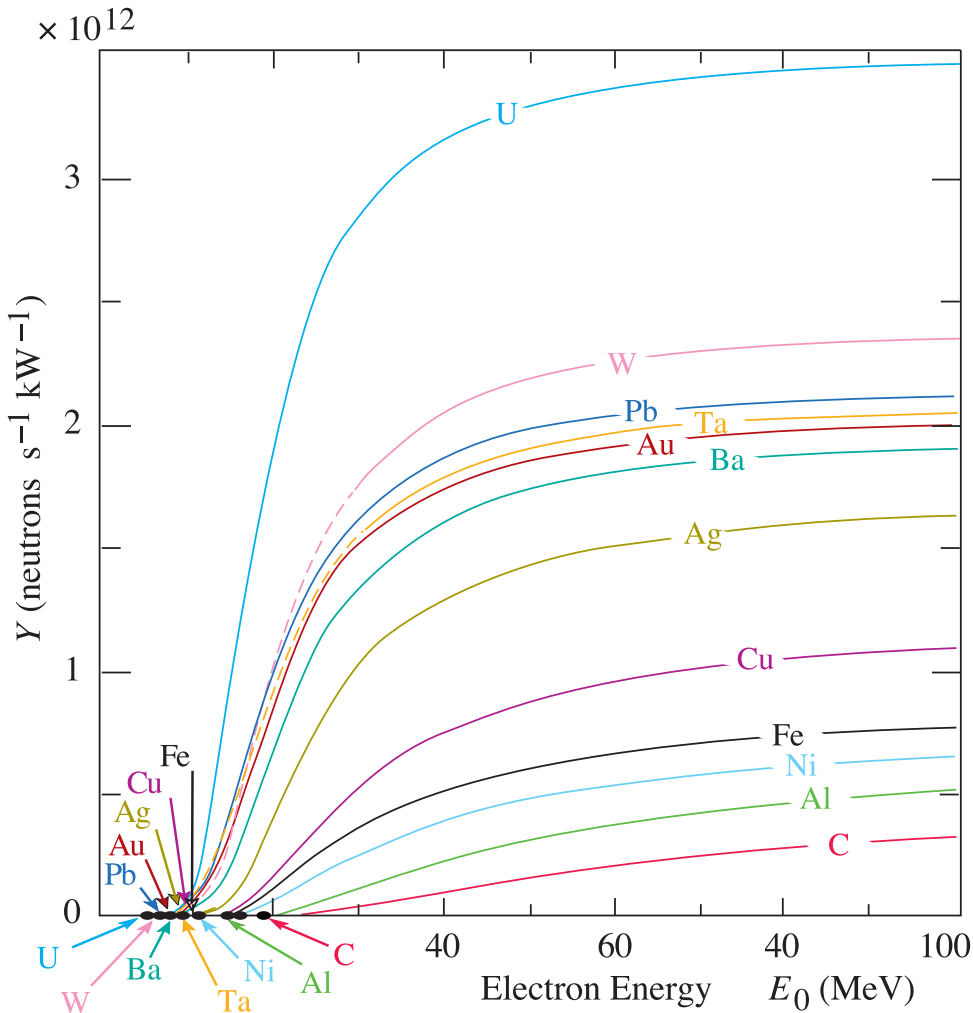
Figure 37.2: Neutron yields from semi-infinite targets per kW of electron beam power, as a function of the electron beam energy, disregarding target self-shielding [7].

a thick copper target. The comparison of these spectra with those for an electron beam of the same energy reflects the difference in the hadronic cross sections between photons and hadrons above a few 100 MeV. Differences are increasing towards lower energies because of different interaction mechanisms. Furthermore, the slight shift in energy above about 100 MeV follows from the fact that the energies of the interacting photons are lower than 25 GeV. Apart from this the shapes of the two spectra are similar.

The neutron-attenuation length is shown in Fig. 37.4 for concrete and mono-energetic broad-beam conditions. As can be seen in the figure it reaches a value of about 117 g/cm^2 above 200 MeV. As the cascade through thick shielding is carried by particles with energies between about 100 MeV and 300 MeV (in this energy range non-elastic cross sections are at minimum and are dominated by quasi-elastic processes leading to low attenuation) this value is equal to the equilibrium attenuation length for particles emitted at 90 degrees in concrete.
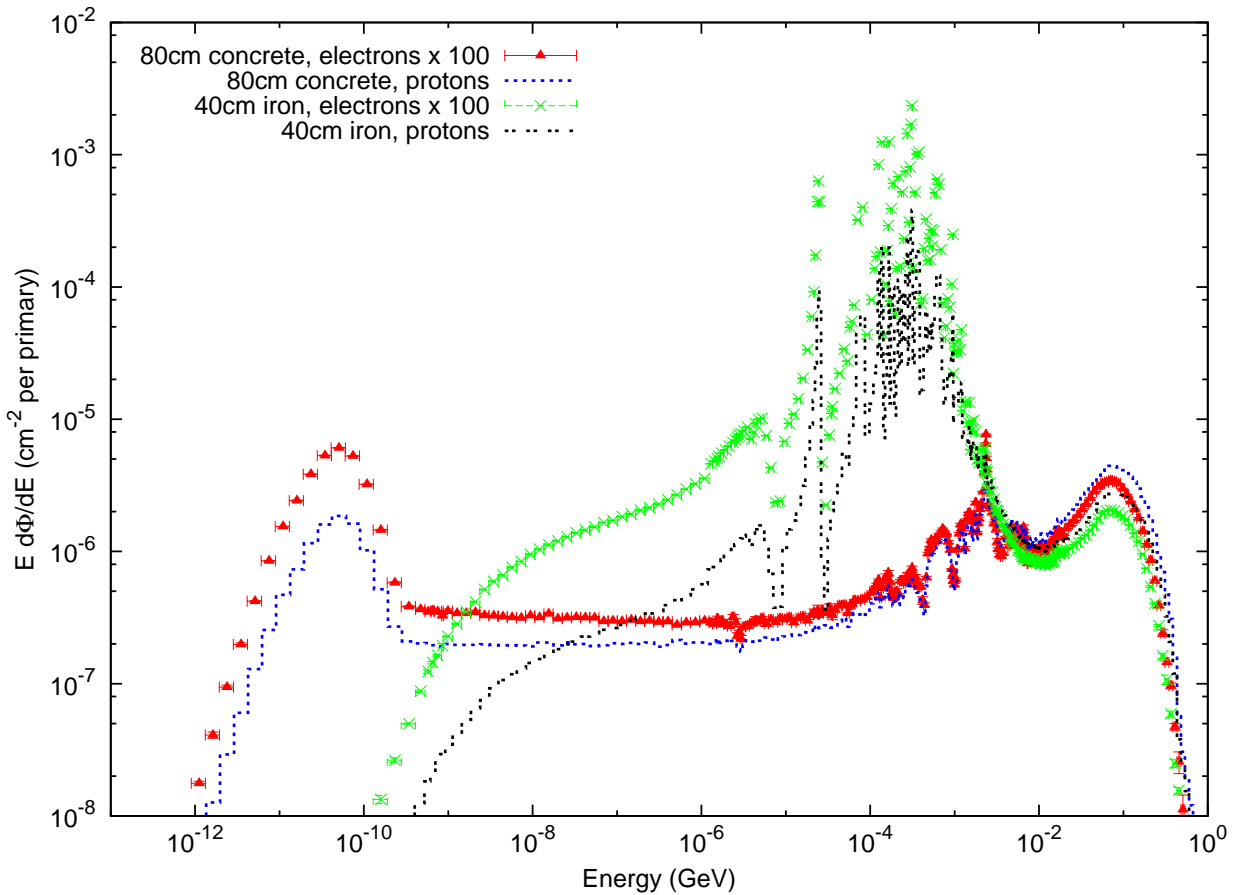
Figure 37.3: Neutron energy spectra calculated with the FLUKA code [8,9] from 25 GeV proton and electron beams on a thick copper target. Spectra are evaluated at 90° to the beam direction behind 80 cm of concrete or 40 cm of iron. All spectra are normalized per beam particle. In addition, spectra for electron beam are multiplied by a factor of 100.

37.5. Photon sources

The dose equivalent rate in tissue (in mSv/h) from a gamma point source emitting one photon of energy E (in MeV) per second at a distance of 1 m is $4.6 \times 10^{-9} \, \mu_{en}/\rho \, E$, where μ_{en}/ρ is the mass energy absorption coefficient. The latter has a value of $0.029 \pm 0.004 \text{ cm}^2/\text{g}$ for photons in tissue over an energy range between 60 keV and 2 MeV (see Ref. 12 for tabulated values).

Similarly, the dose equivalent rate in tissue (in mSv/h) at the surface of a semi-infinite slab of uniformly activated material containing 1 Bq/g of a gamma emitter of energy E (in MeV) is $2.9 \times 10^{-4} \, R_\mu \, E$, where R_μ is the ratio of the mass energy absorption coefficients of the photons in tissue and in the material.
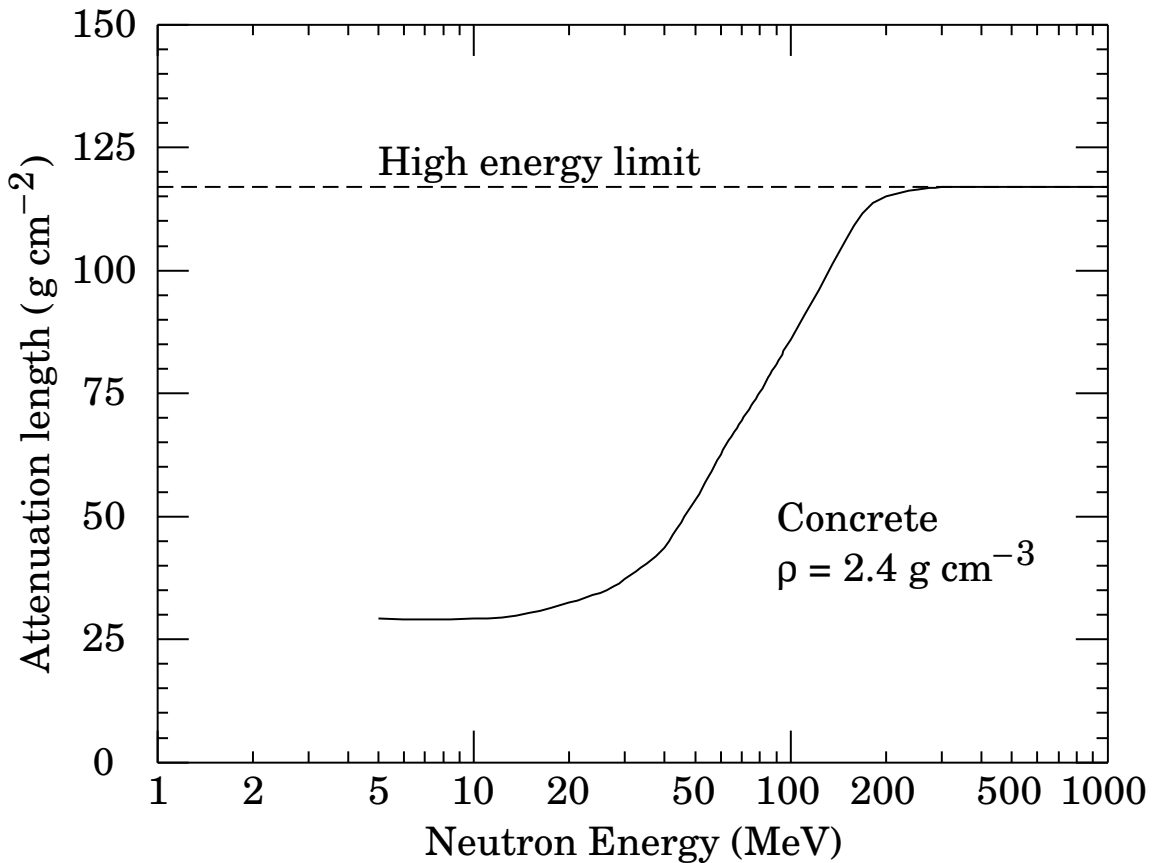
Figure 37.4: The variation of the attenuation length for mono-energetic neutrons in concrete as a function of neutron energy [10].

37.6. Accelerator-induced radioactivity

Typical medium- and long-lived activation products in metallic components of accelerators are ^{22}Na, ^{46}Sc, ^{48}V, ^{51}Cr, ^{54}Mn, ^{55}Fe, ^{59}Fe, ^{56}Co, ^{57}Co, ^{58}Co, ^{60}Co, ^{63}Ni and ^{65}Zn. Gamma-emitting nuclides dominate doses by external irradiation at longer decay times (more than one day) while at short decay times β^+ emitters are also important (through photons produced by β^+ annihilation). Due to their short range, β^- emitters are relevant, for example, only for dose to the skin and eyes or for doses due to inhalation or ingestion. Fig. 37.5 and Fig. 37.6 show the contributions of gamma and β^+ emitters to the total dose rate at 12.4 cm distance to a copper sample [13]. The sample was activated by the stray radiation field created by a 120 GeV mixed hadron beam dumped in a copper target during about 8 hours at intensities between $10^7 - 10^8$ hadrons per second. Typically, dose rates at a certain decay time are mainly determined by radionuclides having a half-life of the order of the decay time. Extended irradiation periods might be an exception to this general rule as in this case the activity of long-lived nuclides can build up sufficiently so that it dominates that one of short-lived even at short cooling times.

Activation in concrete is dominated by ^{24}Na (short decay times) and ^{22}Na (long decay

times). Both nuclides can be produced either by low-energy neutron reactions on the sodium-component in the concrete or by spallation reactions on silicon, calcium and other constituents such as aluminum. At long decay times nuclides of radiological interest in activated concrete can also be ^{60}Co, ^{152}Eu, ^{154}Eu and ^{134}Cs, all of which produced by (n,γ)-reactions with traces of natural cobalt, europium and cesium, Thus, such trace elements might be important even if their content in concrete is only a few parts per million or less by weight.

The explicit simulation of radionuclide production with general-purpose Monte Carlo codes has become the most commonly applied method to calculate induced radioactivity and its radiological consequences [13](see also Sec. 37.8). They are complemented by analytical codes based on folding particle fluence spectra with nuclide production cross sections. ActiWiz [14,15] is an example of such a code targeting the domain of radiological characterization and material optimization. It allows for calculating nuclide inventories by convolution of fluence spectra with nuclide production data for 85 chemical elements and arbitrary compounds from threshold to an energy of 100 TeV.
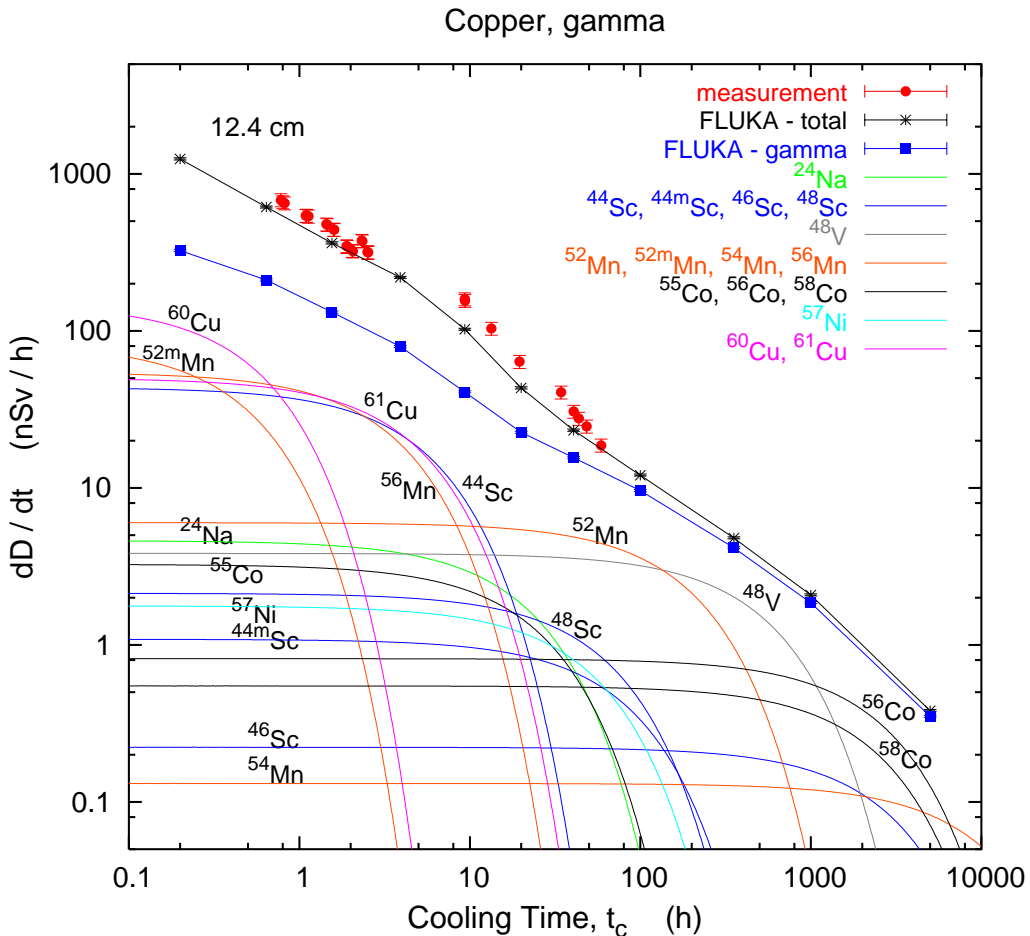

Figure 37.5: Contribution of individual gamma-emitting nuclides to the total dose rate at 12.4 cm distance to an activated copper sample [13].
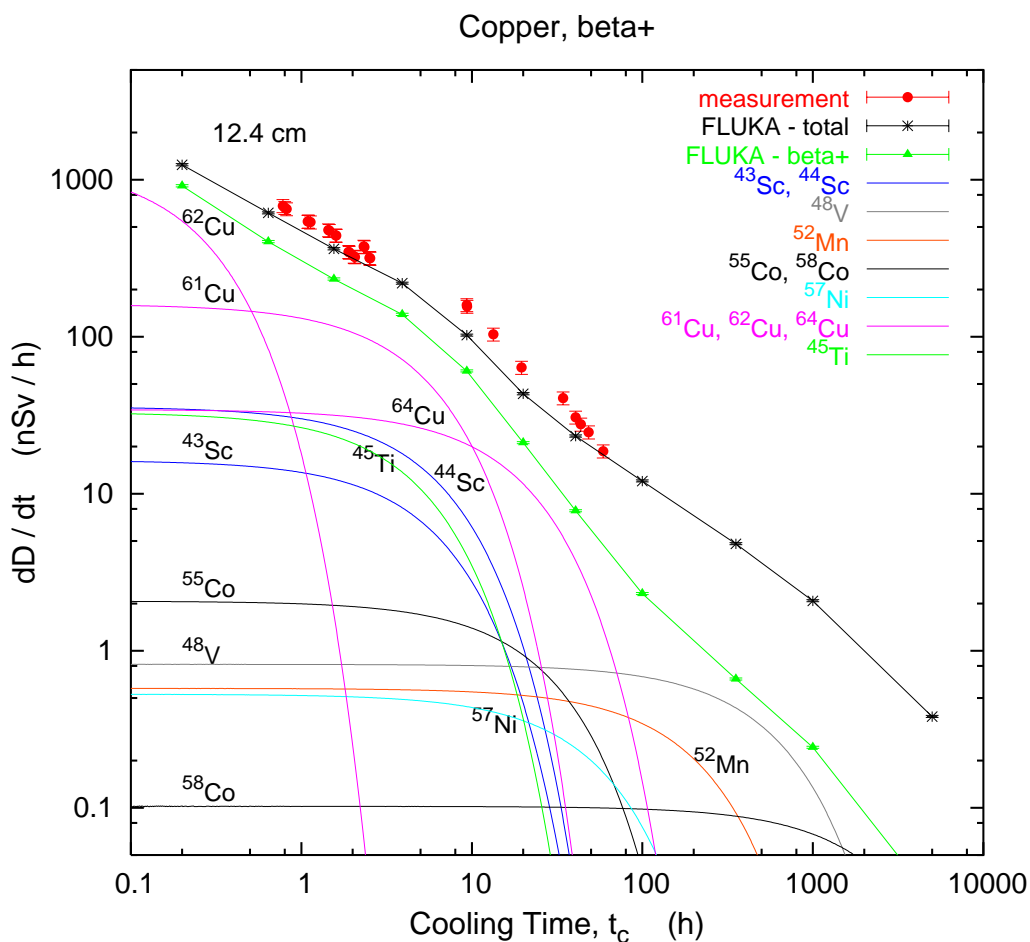
Figure 37.6: Contribution of individual positron-emitting nuclides to the total dose rate at 12.4 cm distance to an activated copper sample [13].

37.7. Radiation protection instrumentation

The capacity to distinguish and measure the high-LET (mostly neutrons) and the low-LET components (photons, electrons, muons) of the radiation field at workplaces is of primary importance to evaluate the exposure of personnel. At proton machines the prompt dose equivalent outside a shield is mainly due to neutrons, with some contribution from photons and, to a minor extent, charged particles. At high-energy electron accelerators the dominant stray radiation during operation consists of high-energy neutrons, because the shielding is normally thick enough to absorb most of the bremsstrahlung photons. Most of the personnel exposure at accelerator facilities is often received during maintenance interventions, and is due to gamma/beta radiation coming from residual radioactivity in accelerator components.

Radiation detectors used both for radiation surveys and area monitoring are normally calibrated in ambient dose equivalent $H^*(10)$.

37.7.1.   *Neutron detectors* :

• **Rem counters:** A rem counter [16] is a portable detector consisting of a thermal neutron counter embedded in a polyethylene moderator, with a response function that approximately follows the curve of the conversion coefficients from neutron fluence to $H^*(10)$ over a wide energy range. Conventional rem counters provide a response to neutrons up to approximately 10-15 MeV, extended-range units are heavier as they include a high-A converter but correctly measure $H^*(10)$ up to several hundred MeV [17].

• **Bonner Sphere Spectrometer (BSS):** A BSS [18] is made up of a thermal neutron detector at the centre of moderating spheres of different diameters made of polyethylene (PE) or a combination of PE and a high-A material to enhance its response to high energy neutrons (similar to rem counters). Each sphere has a different response function versus neutron energy, and the neutron energy, at which the sensitivity peaks, increases with sphere diameter. The energy resolution of the system is rather low but satisfactory for radiation protection purposes. The neutron spectrum is obtained by unfolding the experimental counts of the BSS with its response matrix by a computer code that is often based on an iterative algorithm. BSS exist in active (using ^{3}He or BF$_3$ proportional counters or ^{6}LiI scintillators) and passive versions (using CR-39 track detectors or LiF), for use *e.g.* in strongly pulsed fields. With ^{3}He counters the discrimination with respect to gamma rays and noise is excellent.

• **Bubble detectors:** A bubble detector [19] is a dosimeter based on a super-heated emulsion (super-heated droplets suspended in a gel) contained in a vial and acting as a continuously sensitive, miniature bubble chamber. The total number of bubbles evolved from the radiation-induced nucleation of drops gives an integrated measure of the total neutron exposure. Various techniques exist to record and count the bubbles, *e.g.*, visual inspection, automated reading with video cameras or acoustic counting. Bubble detectors are insensitive to low-LET radiation. Super-heated emulsions are used as personal, area and environmental dosimeters, as well as neutron spectrometers.

• **Track etched detectors:** Track etched detectors (TEDs) [20] are based on the preferential dissolution of suitable, mostly insulator, materials along the damage trails of charged particles of sufficiently high-energy deposition density. The detectors are effectively not sensitive to radiation which deposits the energy through the interactions of particles with low LET. These dosimeters are generally able to determine neutron ambient dose equivalent down to around 100 μSv. They are used both as personal dosimeters and for area monitoring, *e.g.*, in BSS.

37.7.2.   *Photon detectors* [21] :

• **GM counters:** Geiger Müller (GM) counters are low cost devices and simple to operate. They work in pulse mode and since they only count radiation-induced events, any spectrometric information is lost. In general they are calibrated in terms of air kerma, for instance in a ^{60}Co field. The response of GM counters to photons is constant within 15% for energies up to 2 MeV and shows considerable energy dependence above.

• **Ionization chambers:** Ionization chambers are gas-filled detectors used both as hand-held instruments (*e.g.*, for radiation surveys) and environmental monitors. They are normally operated in current mode although pulse-mode operation is also possible. They

possess a relatively flat response to a wide range of X- and gamma ray energies (typically from 10 keV to several MeV), can measure radiation over a wide intensity range and are capable of discriminating between the beta and gamma components of a radiation field (by use of, *e.g.*, a beta window). Pressurized ion chambers (filled, *e.g.*, with Ar or H gas to several tens of bars) are used for environmental monitoring applications. They have good sensitivity to neutrons and charged hadrons in addition to low LET radiation (gammas and muons), with the response function to the former being strongly non-linear with energy.

• **Scintillators:** Scintillation-based detectors are used in radiation protection as hand-held probes and in fixed installations, *e.g.*, portal monitors. A scintillation detector or counter is obtained coupling a scintillator to an electronic light sensor such as a photomultiplier tube (PMT), a photodiode or a silicon photomultiplier (SiPM). There is a wide range of scintillating materials, inorganic (such as CsI and BGO), organic or plastic; they find application in both photon dosimetry and spectrometry.

37.7.3. *Operation in pulsed radiation fields* :

There are many practical situations with particle accelerators used for scientific, industrial and medical applications where the time structure of the stray radiation limits the use of active monitors. Pulsed neutron and gamma fields may be present because of beam losses at, *e.g.*, targets, collimators and beam dumps. The time duration of a single burst can range from a few ns to about 1 ms with a typical repetition rate in the range 0.1–100Hz. Conventional detectors generally suffer from dead time effects and have strong limitations in the measurements of pulsed fields. Severe under response has been observed, *e.g.*, in commercial rem counters, with tremendous underestimation of the ambient dose equivalent, $H^*(10)$, up to three orders of magnitude. The common techniques used to correct the response of radiation detectors which include dead-time corrections operate properly in a steady-state radiation field, whereas it is much more difficult to cope with dead time losses in a pulsed radiation field of unknown time structure and burst dose. Generally speaking the monitoring instrumentation must be chosen on the basis of the knowledge of the radiation field. Detectors with specifically designed electronics must be employed in pulsed field conditions, such as the recently developed LUPIN [22] in place of conventional rem counters for neutrons. If real-time monitoring is not required, passive detectors or dosimeters such as TEDs mentioned in Sec. 37.7.1 or LiF mentioned in Sec. 37.7.4 can be employed, as they are insensitive to the time structure of the radiation.

37.7.4. *Personal dosimeters* :

Personal dosimeters, calibrated in $H_p(10)$, are worn by persons exposed to ionizing radiation for professional reasons to record the dose received. They are typically passive detectors, either film, track etched detectors, ^{6}Li/^{7}Li-based dosimeters (*e.g.* LiF), optically stimulated luminescence (OSL) or radiophotoluminescence detectors (RPL) but semi-active dosimeters using miniaturized ion-chambers also exist.

Electronic personal dosimeters are small active units for on-line monitoring of individual exposure, designed to be worn on the body. They can give an alarm on both the integral dose received or dose rate once a pre-set threshold is exceeded.

37.8.   Monte Carlo codes for radiation protection studies

The use of general-purpose particle interaction and transport Monte Carlo codes is often the most accurate and efficient choice for assessing radiation protection quantities at accelerators. Due to the vast spread of such codes to all areas of particle physics and the associated extensive benchmarking with experimental data, the modeling has reached an unprecedented accuracy. Furthermore, most codes allow the user to simulate all aspects of a high energy particle cascade in one and the same run: from the first interaction of a TeV nucleus over the transport and re-interactions (hadronic and electromagnetic) of the produced secondaries, to detailed nuclear fragmentation, the calculation of radioactive decays and even of the electromagnetic shower caused by the radiation from such decays. A brief account of the codes most widely used for radiation protection studies at high energy accelerators is given in the following.

• **FLUKA [8,9]:** FLUKA is a general-purpose particle interaction and transport code. It comprises all features needed for radiation protection, such as detailed hadronic and nuclear interaction models up to 10 PeV, full coupling between hadronic and electromagnetic processes and numerous variance reduction options. The latter include weight windows, region importance biasing, and leading particle, interaction, and decay length biasing (among others). The capabilities of FLUKA are unique for studies of induced radioactivity, especially with regard to nuclide production, decay, and transport of residual radiation. In particular, particle cascades by prompt and residual radiation are simulated in parallel based on the microscopic models for nuclide production and a solution of the Bateman equations for activity build-up and decay.

• **GEANT4 [23,24,25]:** GEANT4 is an object-oriented toolkit consisting of a kernel that provides the framework for particle transport, including tracking, geometry description, material specifications, management of events and interfaces to external graphics systems. The kernel also provides interfaces to physics processes. It allows the user to freely select the physics models that best serve the particular application needs. Implementations of interaction models exist over an extended range of energies, from optical photons and thermal neutrons to high-energy interactions required for the simulation of accelerator and cosmic ray experiments. To facilitate the use of variance reduction techniques, general-purpose biasing methods such as importance biasing, weight windows, and a weight cut-off method have been introduced directly into the toolkit. Other variance reduction methods, such as leading particle biasing for hadronic processes, come with the respective physics packages.

• **MARS15 [26,27,28]:**   The MARS15 code system is a set of Monte Carlo programs for the simulation of hadronic and electromagnetic cascades. It covers a wide energy range: 1 keV to 100 TeV for muons, charged hadrons, heavy ions and electromagnetic showers; and 0.00215 eV to 100 TeV for neutrons. Hadron-nucleus interactions as well as practically all other strong, weak and electromagnetic interactions in the entire energy range can be simulated either inclusively or exclusively. MARS15 uses ENDFB-VII nuclear data to handle interactions of neutrons with energies below 14 MeV. Several variance reduction techniques, such as weight windows, particle splitting, and Russian roulette, are available in MARS15. A tagging module allows one to tag the origin of a given signal for source term or sensitivity analyses. The geometry module allows either

a basic solid body representation option or a ROOT-based powerful engine. Further features of MARS15 include a MAD-MARS merge for a convenient creation of accelerator models and multi-turn tracking and cascade simulation in accelerator and beamline lattices.

- **MCNP6 [29,30]:** MCNP6 is the latest version of the Monte Carlo N-Particle transport (MCNP) family of neutron interaction and transport codes and, therefore, features one of the most comprehensive and detailed descriptions of the related physical processes. It transports 37 different particle types, including ions and electromagnetic particles. The neutron interaction and transport modules use standard evaluated data libraries mixed with physics models where such libraries are not available. The transport is continuous in energy. MCNP6 contains one of the most powerful implementations of variance reduction techniques. Spherical mesh weight windows can be created by a generator in order to focus the simulation time on certain spatial regions of interest. In addition, a more generalized phase space biasing is also possible through energy- and time-dependent weight windows. Other biasing options include pulse-height tallies with variance reduction and criticality source convergence acceleration.

- **PHITS [31,32]:** The Particle and Heavy-Ion Transport code System PHITS was among the first general-purpose codes to simulate the transport and interactions of heavy ions in a wide energy range, from 10 MeV/nucleon to 100 GeV/nucleon. It is based on the high-energy hadron transport code NMTC/JAM that was extended to heavy ions. The transport of low-energy neutrons employs cross sections from evaluated nuclear data libraries such as ENDF and JENDL below 20 MeV. Electromagnetic interactions are simulated based on the ITS code in the energy range between 1 keV and 100 MeV for electrons and positrons and between 1 keV and 100 GeV for photons. Several variance reduction techniques, including weight windows and region importance biasing, are available in PHITS.

References:

1. International Commission on Radiation Units and Measurements, *Fundamental Quantities and Units for Ionizing Radiation*, ICRU Report 60 (1998).
2. ICRP, 2010. *Conversion Coefficients for Radiological Protection Quantities for External Radiation Exposures*, ICRP Publication 116, Annals of the ICRP 40(2-5).
3. ICRP Publication 103, *The 2007 Recommendations of the International Commission on Radiological Protection*, Annals of the ICRP, Elsevier (2007).
4. M. Pelliccioni, Radiation Protection Dosimetry **88**, 279 (2000).
5. E. Pochin, *Nuclear Radiation: Risks and Benefits*, Clarendon Press, Oxford, 1983.
6. United Nations, *Report of the United Nations Scientific Committee on the Effect of Atomic Radiation*, General Assembly, Official Records A/63/46 (2008).
7. W.P. Swanson, *Radiological Safety Aspects of the Operation of Electron Linear Accelerators*, IAEA Technical Reports Series No. 188 (1979).
8. A. Ferrari, *et al.*, FLUKA, A Multi-particle Transport Code (Program Version 2005), CERN-2005-010 (2005), `www.fluka.org`.
9. T.T. Böhlen, *et al.*, The FLUKA code: Developments and Challenges for High Energy and Medical Applications, Nuclear Data Sheets **120**, 211 (2014).

10. R.H. Thomas and G.R. Stevenson, *Radiological Safety Aspects of the Operation of Proton Accelerators,* IAEA Technical Report Series No. 283 (1988).

11. T.A. Gabriel, *et al.*, Nucl. Instrum. Methods **A338**, 336 (1994).

12. `http://physics.nist.gov/PhysRefData/XrayMassCoef/cover.html`.

13. S. Roesler, *et al.*, "Simulation of Remanent Dose Rates and Benchmark Measurements at the CERN-EU High Energy Reference Field Facility," in *Proceedings of the Sixth International Meeting on Nuclear Applications of Accelerator Technology,* San Diego, CA, 1-5 June 2003, 655–662 (2003).

14. C. Theis and H. Vincke, "The use of ActiWiz in operational radiation protection," in *Proceedings of the Twelfth Meeting of Task-Force on Shielding Aspects of Accelerators, Targets and Irradiation Facilities of Accelerator Technology, SATIF12* FNAL, 28-30 April 2014, Nuclear Science Report NEA/NSC/R 3, (2015).

15. C. Theis and H. Vincke, "ActiWiz3 an overview of the concepts, architecture and new features," CERN Technical Note CERN-RP-2016-117-REPORTS-TN (2016), `actiwiz.web.cern.ch`.

16. I.O. Andersson and J. Braun, A neutron rem counter with uniform sensitivity from 0.025 eV to 10 MeV in *Proceedings of the IAEA Symposium on Neutron dosimetry,* IAEA, Vienna, Vol. II, 87–95, (1963).

17. C. Birattari, *et al.*, Radiation Protection Dosimetry **76**, 135 (1998).

18. R.L. Bramblett, R.I. Ewing and T.W. Bonner, Nuclear Instruments and Methods **9**, 1 (1960).

19. F. d'Errico, Nucl. Instrum. Methods **B184**, 229 (2001).

20. K. Becker, Dosimetric applications of track etching, in *Topics in Radiation Dosimetry* Ed. F.H. Attix, Academic Press, London, 79–143, (1972).

21. G.F. Knoll, *Radiation detection and measurements,* Wiley (2010).

22. M. Caresana, *et al.*, A new version of the LUPIN detector: Improvements and latest experimental verification, Review of Scientific Instruments **85**, 065102 (2014).

23. S. Agostinelli, *et al.*, Nucl. Instrum. Methods **A506**, 250 (2003).

24. J. Allison, *et al.*, IEEE Transactions on Nuclear Science **53**, 270 (2006).

25. J. Allison, *et al.*, Nucl. Instrum. Methods **A835**, 186 (2016), `geant4.cern.ch`.

26. N.V. Mokhov, S.I. Striganov, MARS15 Overview *Proceedings of the Hadronic Shower Simulation Workshop 2006,* Fermilab 6–8 September 2006, M. Albrow, R. Raja, eds., *AIP Conference Proceeding 896*, 50–60, (2007).

27. N.V. Mokhov, MARS Code System, Version 15 (2016), `mars.fnal.gov`.

28. N.V. Mokhov, *et al.*, Prog. Nucl. Sci. Technol. **4**, 496 (2014).

29. D. Pelowitz, *et al.*, Los Alamos National Laboratory report, LA-CP-14-00745 (2014), `mcnp.lanl.gov`.

30. J.T. Goorley, *et al.*, Nuclear Technology **180**, 298 (2012).

31. T. Sato, *et al.*, Journal of Nuclear Science and Technology **50**, 913 (2013).

32. T. Sato, *et al.*, PHITS Particle and Heavy Ion Transport code System, Version 2.88 (2017), `phits.jaea.go.jp`.